Model-based detector and extraction of weak signal frequencies from chaotic data

Cangtao Zhou,[1,2,a)] Tianxing Cai,[3] Choy Heng Lai,[4,5] Xingang Wang,[1,5] and Ying-Cheng Lai[6]

[1]*Temasek Laboratories, National University of Singapore, Singapore 117508*
[2]*Center for Applied Physics and Technology, Peking University, Beijing 100871, People's Republic of China*
[3]*College of Jia Hua, Beijing Technology and Business University, Beijing 101118, People's Republic of China*
[4]*Department of Physics, National University of Singapore, Singapore 117542*
[5]*Beijing–Hong Kong–Singapore Joint Centre for Nonlinear & Complex Systems (Singapore), National University of Singapore, Singapore 117542*
[6]*Department of Electrical Engineering and Department of Physics and Astronomy, Arizona State University, Tempe, Arizona 85278, USA*

Detecting a weak signal from chaotic time series is of general interest in science and engineering. In this work we introduce and investigate a signal detection algorithm for which chaos theory, nonlinear dynamical reconstruction techniques, neural networks, and time-frequency analysis are put together in a synergistic manner. By applying the scheme to numerical simulation and different experimental measurement data sets (Hénon map, chaotic circuit, and NH_3 laser data sets), we demonstrate that weak signals hidden beneath the noise floor can be detected by using a model-based detector. Particularly, the signal frequencies can be extracted accurately in the time-frequency space. By comparing the model-based method with the standard denoising wavelet technique as well as supervised principal components analysis detector, we further show that the nonlinear dynamics and neural network-based approach performs better in extracting frequencies of weak signals hidden in chaotic time series. © *2008 American Institute of Physics.*
[DOI: 10.1063/1.2827500]

Traditionally, there are basically two kinds of techniques for signal processing. They are time-domain, such as beam forming, and frequency-domain, such as power spectral density, short-time Fourier transform, Wigner–Ville distribution, etc. In nonlinear processing of physical signals, a third kind of technique, i.e., phase-space reconstruction and analysis, has become common. The conceptual breakthrough, together with the availability of sensing and data processing technologies, has generated an enormous interest in the application of nonlinear dynamics. Nonlinear signal processing methods, which analyze signals from the dynamical perspective, offer an alternative paradigm. However, detecting signals hidden beneath the noise floor is still a challenging task. As the signal-to-noise ratio falls below unity, false alarms and detection misses become serious problems. Furthermore, to satisfy real-time requirements, detection schemes that are computationally intensive do not enjoy widespread adoption. In this work we introduce a small target detection strategy based on chaos, phase-space embedding technique, neural networks, and power spectral analyses. The approaches proposed are applicable to the problem of nonlinear modeling and detection. By analyzing different experimental measurement data sets, we demonstrate that the frequencies of signals hidden in the chaotic data can be extracted accurately.

I. INTRODUCTION

Signal detection and separation are problems commonly encountered in science and engineering.[1–16] Conventional signal detection techniques[17] based on statistical decision theory typically approach the problem via the methodology of hypothesis testing. Specifically, a choice is made between two hypotheses through the use of some decision-making criterion. The decision-making problem is usually solved by Bayes' hypothesis-testing procedure, with some statistical assumptions or parametric characterizations of noise. The problem becomes more challenging when a target signal is much weaker, say, with a less-than-unity signal-to-noise ratio (SNR), than the background chaotic signal or noise. Most importantly, the unwanted background noise could be generated by an unknown nonlinear dynamical mechanism, rendering the assumptions of linearity, Gaussianity, and stationarity, which are typically made in the standard statistical approach to signal processing, invalid.

Recently, nonlinear dynamical modeling[1–3,15,16,18,19] has been combined with other techniques such as artificial neural network[20] (ANN) and time-frequency analysis[21] to give rise to a class of algorithms for signal detection. Research has shown that different ANNs,[8,9] such as principal components

a)Permanent address: Institute of Applied Physics and Computational Mathematics, P.O. Box 8009, Beijing 100088, People's Republic of China.

analysis, multilayer perceptron and radial basis function (RBF) networks, etc., are able to perform the task of detecting signals in time series data contaminated by nonlinear and nonstationary background noise.

Dynamical modeling consists of matching the behavior of a computational system to that exhibited by the measurement data obtained from a physical system. If the dynamical system is linear, an autoregressive moving average (ARMA) model is sufficient. However, for nonlinear systems, ARMA models are not sufficient and alternative models must be used. Many modeling techniques can be used to solve problems of this type; for example, rational polynomial, multilayer perceptrons, RBF and support vector neural networks, etc.[8–10]

In this work, we use a RBF neural network to build our underlying dynamical equations. The signal-detection problem is solved by using a model-based algorithm. Theoretically, such a model-based detector can yield a good detection performance if the interference results from a chaotic dynamical system. In experimental environments, however, it is practically impossible to separate the deterministic component of a measured signal from random noise. In this case, a model-based method can be quite effective, as we shall demonstrate in this paper. We first discuss a nonlinear dynamical modeling scheme based on phase-space reconstruction,[18,19,22] RBF neural networks,[20,23] and frequency spectrum analysis.[21] The model[8–10] is used to design a chaos-based signal enhancement detection strategy. Behaviors of this detector are studied by using computer generated chaotic data. We then apply the detection algorithm to several experimental measurement data sets, such as chaotic circuit and NH_3 laser data.

II. MODEL-BASED DETECTOR

We first introduce and review a model-based detector. RBF networks are a special class of feed-forward networks that consist of three different layers:[20] an input layer, one hidden layer, and an output layer. An important property of RBF networks is that the transformation from the input layer to the hidden layer is nonlinear; however, the mapping from the hidden layer to the output layer is linear. The basic form of a RBF model can be written as[20]

$$f(x) = \sum_{i=1}^{N_c} w_i h_i(x), \qquad (1)$$

where f is expressed as a linear combination of a set of N_c fixed basis functions h_i, and w_i are linear coefficients. A convenient choice for h_i is the Gaussian radial function

$$h(x) = \exp\left[-\frac{(x - x^c)^2}{r^2}\right], \qquad (2)$$

with center x^c and radius r. By using a training set

$$\Im = \{(x_i, \hat{y}_i)\}_{i=1}^N, \qquad (3)$$

where N is the length of the data points, one obtains the optimal weight vector[8]

$$W = (H^T H + \lambda I_{N_c})^{-1} H^T \hat{y}. \qquad (4)$$

Note that I is the $N_c \times N_c$ unit matrix, while H is the $N \times N_c$ design matrix calculated in terms of the RBFs in Eq. (2). In Eq. (4), the regularization parameter λ is associated with low values of the prediction error. To choose a suitable regularization parameter is important for avoiding over-fits of the underlying equation to noisy data,[9] and there are many techniques,[23] for example, Bayesian information criterion (BIC) and generalized cross-validation, etc., to determine the optimal regularization parameter.

Since all the model selection criteria depend nonlinearly on λ, a method of nonlinear optimization is needed. One could use any of the standard techniques for this, such as the Newton method. Alternatively, one can exploit the fact that when the derivative of the prediction error is set to zero, the resulting equation according to BIC can be manipulated so that λ can be expressed as follows:[23]

$$\lambda = \frac{\hat{y}^T P^2 \hat{y} \, \mathrm{Tr}(A^{-1} - \lambda A^{-2})}{W^T A^{-1} W} \frac{N \ln(N)}{2(N - \gamma)\{N + [\ln(N) - 1]\gamma\}}, \qquad (5)$$

where $P = I - H A^{-1} H^T$ is the projection matrix, $A^{-1} = (H^T H + \lambda I)^{-1}$ is the variance matrix, and $\gamma = N - \mathrm{Tr}(P)$ denotes the effective number of parameters. Note that Eq. (5) is not a solution; it is a re-estimation formula because the right-hand side depends on λ. To use it, an initial value of λ is chosen[24] and used to calculate a value for the right-hand side. This leads to a new estimate and the iterative process can continue until satisfactory convergence is achieved. Once the regularization parameter λ is chosen with the knowledge of the training data set (3), one may compute the design matrix H using RBFs and then obtain the optimal vector of weights W that minimizes the mean-squared prediction error.

An important problem concerns how a training set can be built from a single time series of measurement. A simple method for constructing the input-output pairs of the network is to apply the phase-space reconstruction technique. Given a finite time series data $v(n)$, where v is a component of a vector V that represents a variable evolving according to some unknown dynamical system, our goal is to predict the near-future behavior of the time series $v(n)$. This can be done in principle. In particular, Takens embedding theorem[18,19] ensures that, under certain conditions, for almost all time delay τ and for some $m \leq 2D + 1$, where D is the fractal dimension of the attractor and m is the embedding dimension, there is a smooth $g : \mathfrak{R}^m \rightarrow \mathfrak{R}^1$ such that

$$v(n\tau) = g(v((n-1)\tau), \ldots, v((n-m)\tau)). \qquad (6)$$

Comparing Eq. (3) with Eq. (6), we see that the training set (3) can be written in the following form:

$$\Im \equiv \{v(i + (j-1)\tau), v(i + m\tau)\}_{i=1,\ldots,N}^{j=1,\ldots,m}, \qquad (7)$$

where τ is the time delay, and $\{v(k), k = 1, \ldots, N'\}$ with $N' = N + m\tau$ is the observed time series to be analyzed. After the input-output pairs $\Im$ are given, one can proceed to choose an optimal regularization parameter λ by the BIC algorithm (5), and the minimum number of center points by minimizing the mean-squared error (MSE). After obtaining the design matrix H and the weights W of the networks through training, we

form the underlying dynamical model (1), which may be rewritten in the form $f(\mathbf{x}) = HW$.

We now turn to the problem of designing the detection algorithm by using the prediction equation (1). We introduce here a detection strategy[8] rooted in chaos theory. It is based on the existence of at least one positive Lyapunov exponent in the chaotic dynamical system responsible for the generation of an initial chaotic process $v_0(n)$. The basic idea is as follows. Since chaos can be generated in a deterministic nonlinear dynamical system, we may invoke Takens embedding theorem to build a model (1) that represents a reconstruction of the system responsible for generating $v_0(n)$. For a real observed signal $v(n)$ that contains a target signal $s(n)$, the model is no longer suitable as $v(n)$ in general differs from $v_0(n)$. The target signal $s(n)$, however, manifests itself as a perturbation at the output of the model. Mathematically, the difference between the predicted data $f(\mathbf{x})$ and the data $\hat{y}_{\text{meas}}(n)$ may be expressed as

$$
\begin{aligned}
e(n+1) &= f(\mathbf{x}_{\text{meas}}, W) - \hat{y}_{\text{meas}}(n+1) \\
&= f(\mathbf{x}(n) + \mathbf{s}(n)) - [f(\mathbf{x}(n)) + \mathbf{s}(n)] \\
&\propto f(\mathbf{x}(n)) + \partial f / \partial \mathbf{x}(n) \cdot \mathbf{s}(n) - f(\mathbf{x}(n)) - \mathbf{s}(n) \\
&\propto \mathbf{s}(n)(\partial f / \partial \mathbf{x}(n) - 1) \\
&\propto s(n)(e^{\lambda_i n} - 1),
\end{aligned}
\tag{8}
$$

for $i = 1, \ldots, m$, where λ_i is the ith Lyapunov exponent, m is the dimension of the dynamical system, and n gives the index of time series. For a chaotic system, $\lambda_i > 0$ for some i, we thus see that the target signal is enlarged by $e^{\lambda_i n} > 1$ and $e(n) > s(n)$. It should be noted that the linear analysis given in Eq. (8) cannot be used directly to extract the signal component $s(n)$ from a chaotic time series. However, this expression provides the basis of a method to detect the existence of a "weak" signal component. On the one hand, the prediction error e will behave like a random series if the measured data $\hat{y}_{\text{meas}}$ does not contain any signal component. The error source may be the device error and/or the modeling error. Their corresponding error spectra reveal pseudorandom features. When a signal component is present in $\hat{y}_{\text{meas}}$, on the other hand, the prediction error e as defined in Eq. (8) indicates the existence of the enhanced signal component. By analyzing the characteristics of the error series $e(n)$ using, for example, a time-frequency analysis and comparing its spectrum with the spectrum of the original data, $s(n)$ can thus be detected if any new feature in the spectrum of $e(n)$ is observed.

A step-by-step implementation of our model-based detection algorithm is as follows.

- Consider two time series $\{v_0(i), i = 1, \ldots, N_0'\}$ and $\{v(i), i = 1, \ldots, N'\}$. The former labeled with subscript "0" is a time series of the background environment in the absence of target signal, and the latter consists of both the background and the target signal.
- Determine the optimal reconstruction parameters[4–7] (embedding dimension m and time delay τ) based on nonlinear time series analysis techniques Eq. (6). In particular, m can be determined by computing the correlation dimension or

false nearest neighbors, and τ can be given by computing the autocorrelation or mutual information.[18,19]
- With Eqs. (3) and (7), we can reconstruct the input-output pairs of RBF networks using both the training and test data series: $\{x_{i,0}^j, \hat{y}_{i,0}\}$ with $j = 1, \ldots, m$, $i = 1, \ldots, N_0 = N_0' - m\tau$ and $\{x_i^j, \hat{y}_i\}$ with $j = 1, \ldots, m$, $i = 1, \ldots, N = N' - m\tau$.
- Determine the optimal regularization parameter λ using Eq. (5) and the minimum number of the hidden layer by minimizing the prediction error.
- Choose a radial basis function (2) with a suitable width to compute design matrices H_0 and H.
- Obtain the optimal vector W_0 of weights of the network in terms of Eq. (4).
- Using the trained network parameters and test series, we can compute the prediction error between the measured series and the prediction data $e = \hat{y} - HW_0$.
- Analyze the characteristics of the error series e using time-frequency analysis and compare its spectrum with the spectrum of the original data. Any new feature in the spectrum of e is indicative of the presence of the weak target signals.
- Compute the mean-square value $R_e = \Sigma_{i=1}^N (e(i))^2 / N$ and compare R_e with the threshold for a given probability of false alarm. Exceeding the threshold indicates successful detection of the target signal.

III. MODELING, DETECTION, AND ROBUST ANALYSES USING A NUMERICAL EXAMPLE

A. Modeling

As an example, we consider a time series $v(i)(=x(i))$, $i = 1, \ldots, 4000$ generated from the x component of the Hénon map

$$
\begin{aligned}
x(n+1) &= 1 - 1.4x^2(n) + y(n), \\
y(n+1) &= 0.3x(n).
\end{aligned}
\tag{9}
$$

The embedding dimension can be determined from the correlation dimension D_2. For the Hénon data, it is found that $D_2 \approx 1.19$. Thus, the embedding dimension is taken as $m = Ceil(2D_2 + 1) = 3$. To determine the time delay τ, we compute the autocorrelation function and/or mutual information. For this time series, we get $\tau = 1$. Using Eq. (7), we can construct the input-output pairs of the RBF networks. To test the modeling performance, we use the first 2000 points as the training series to model the underlying dynamics, and the second 2000 points for testing purposes.

In order to design the matrix H_0 using the training series, we determine the number of center points required. By applying the minimum MSE value as a modeling criterion, we obtain $N_c = 40$. The center points are randomly chosen from the reconstructed attractor. To get the optimal regularization parameter λ, we use the BIC algorithm. The optimal value is found to be $\lambda \approx 2.81 \times 10^{-12} \sim 0$.

Using the test data set and the underlying equation, we can get one-step prediction data. As shown in Fig. 1(b), the modeling data completely fits the test series, where MSE ≈ 0.0001 is small. We also compute the correlation dimen-
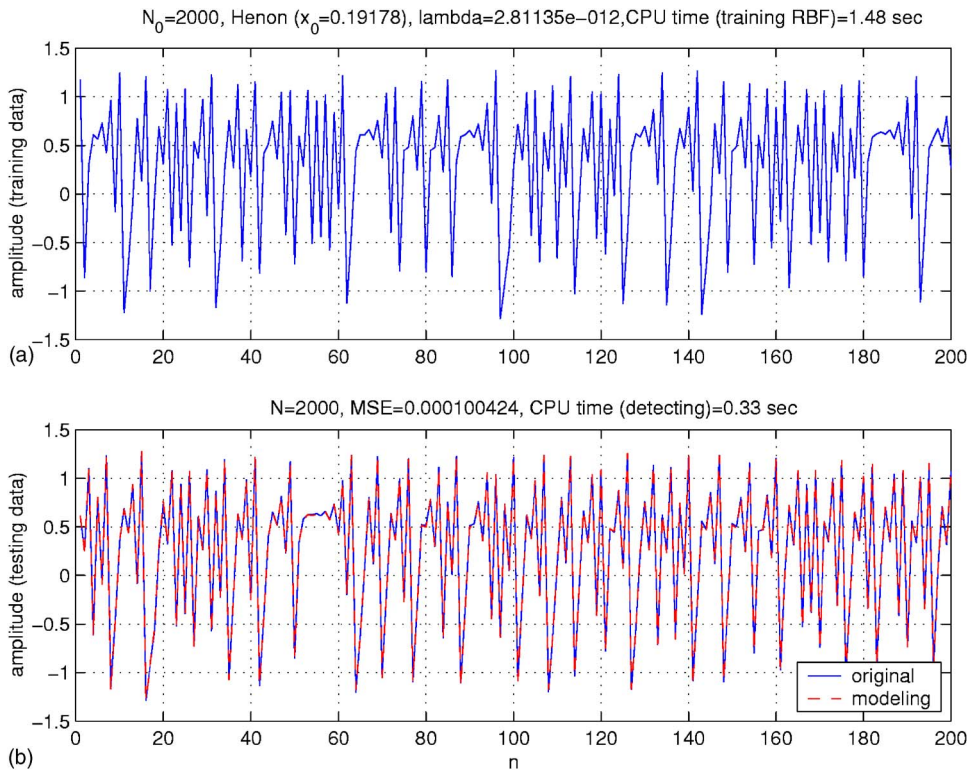
FIG. 1. (Color online) (a) Hénon time series for training RBF networks with $(m, \tau) = (3, 1)$. (b) Hénon time series for testing RBF networks. Solid trace is the original Hénon time series, and the red trace (dashed line) corresponds to one-step prediction data.

sion of the modeling series. Its value is $D_2 \approx 1.24$, which is compatible with the true value of 1.19. Our neural-network-based model is thus suitable for the Hénon chaotic system.

B. Detection and robust analyses

We now illustrate the detection performance of our scheme with the Hénon map. We use the x component of the map and add a two-frequency target signal $s(t_n) = \sin(2\pi f_0 t_n) + 0.8 \sin(3\pi f_0 t_n)$ (f_0 is the fundamental frequency of the signal) to the chaotic data with SNR $= -35$ dB. For such a small value of SNR, Fig. 2 shows that

the signal frequency is completely hidden in the chaotic broadband spectrum. Figures 3(a) and 3(b) show the amplitude spectra of the original Hénon data and the data with hidden target signal. The detection result is given in Fig. 3(c). As expected, two frequencies ($f_0 = 60$ and 90) of the target signal can be correctly extracted.

We have also considered a broadband signal $s(t_n) = \sin[2\pi f_0(1 + 0.05 t_n) t_n]$, as shown in Fig. 4. The signal is immersed completely in the chaotic data. The frequency spectra of the original chaotic signal and the signal with target signal are shown in Figs. 5(b) and 5(a), respectively.
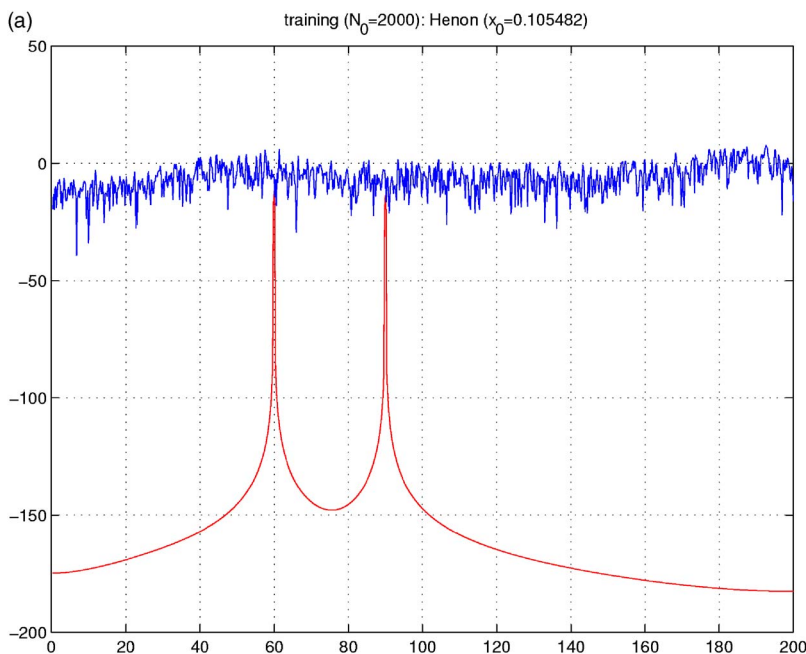

FIG. 2. (Color online) Power spectrum of Hénon chaotic signal and a two-frequency target signal with SNR $= -35$ dB.

training (N_0=2000): Henon (x_0=0.105482)

testing (N=2000):sin(2*pi*60*t)+0.8sin(2*pi*90*t)+Henon (x_0=0.138424) (SNR=−35dB)

detection using RBF (m,del)=(3,1): lambda=6.1639e−012, MSE=0.00169223, CPU time=1.86 sec
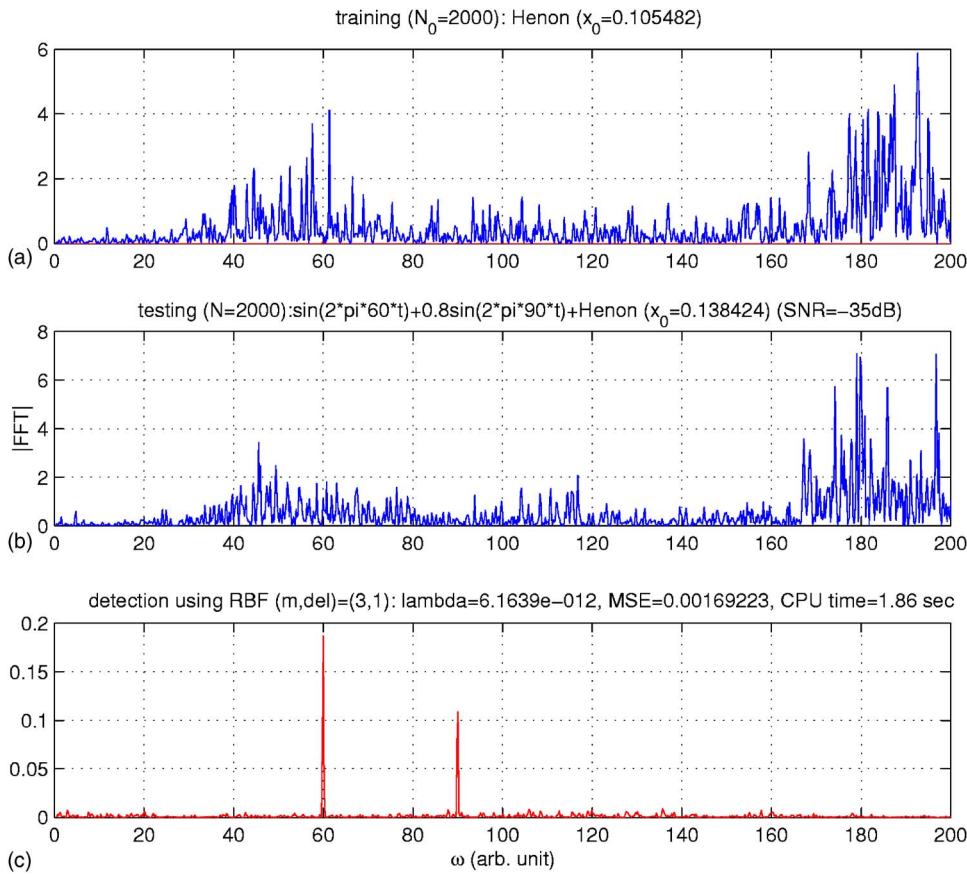
ω (arb. unit)

FIG. 3. (Color online) Frequency spectra of (a) Hénon chaotic signal, (b) mixed Hénon and target signal, and (c) the prediction error. We see that the two frequencies (f_0=60 and 90) of the target signal can be extracted accurately.

Apparently, no signal feature can be found in Fig. 5(b). After using the RBF-based detection algorithm, the spectrum of the signal (in $60 < f_0 < 80$) becomes observable, as shown in Fig. 5(c).

To analyze the robustness of our detection strategy, we have considered the case where Gaussian noise is present in the chaotic signal with several values of chaos-to-noise ratio (CNR).[25] To characterize the tolerance of our scheme to noise, we define a relative MSE:

$$\eta_{mse} = \frac{MSE^{(0)}}{MSE},$$ (10)

where $MSE^{(0)}$ is the mean-squared error between the training data and the corresponding RBF network modeling data, and MSE is the mean-squared error between the test data and the corresponding modeling data. Ensemble statistics are computed for 100 different training and testing data sets, and the regularization parameter is computed by the BIC algorithm
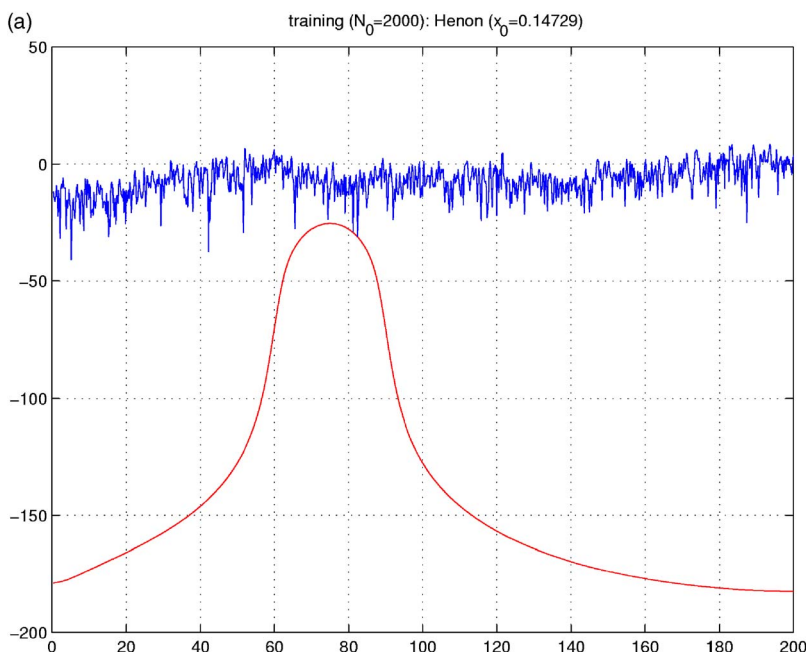

training (N_0=2000): Henon (x_0=0.14729)

FIG. 4. (Color online) Power spectra of the Hénon chaotic signal and a broadband target signal with SNR =−35 dB.
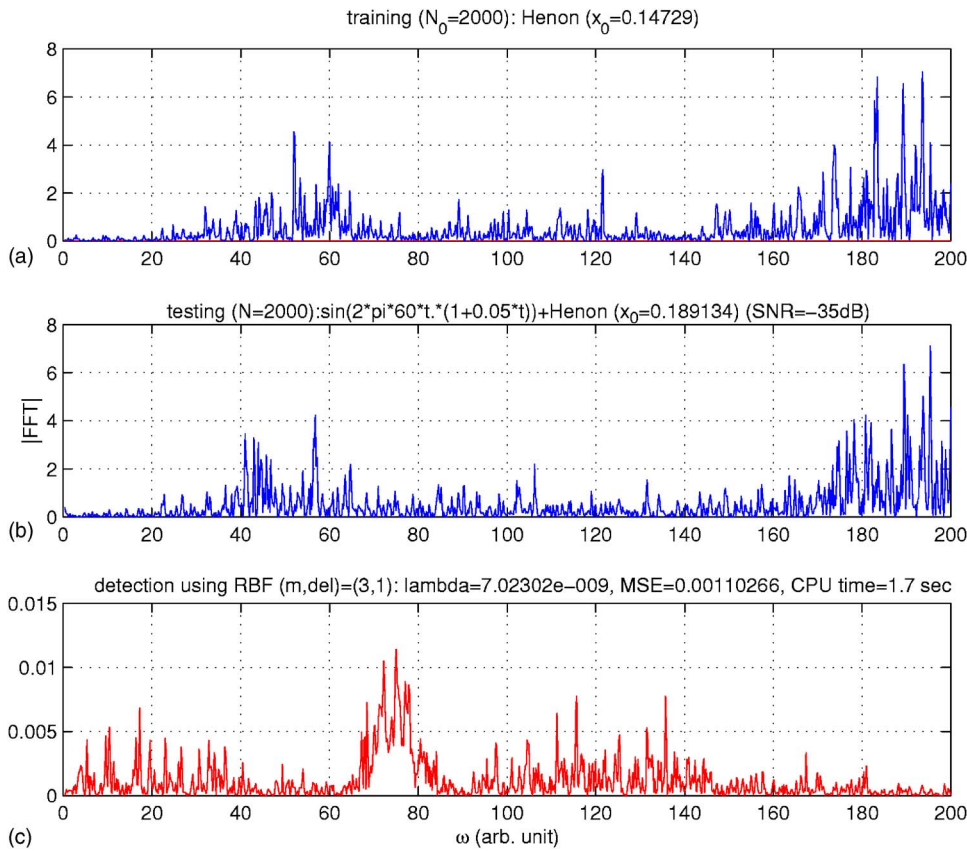
FIG. 5. (Color online) Frequency spectra of (a) Hénon chaotic signal, (b) mixed Hénon chaotic and broadband target signal, and (c) the prediction error.

for each run. Four different CNR values are chosen. For each CNR value, we add three different signal sources; namely, periodic signal, computer-generated broadband signal, and a real speech signal, to the Hénon chaotic time series. The detection results are summarized in Fig. 6, where the shallow

dark line stands for the detection threshold for a given false alarm. If η_{mse} exceeds the threshold, we say that a target is present; otherwise, the scheme fails to detect a target signal. From Fig. 6(a), a case of noise-free Hénon time series, we see that signal detection is possible for very low SNR values
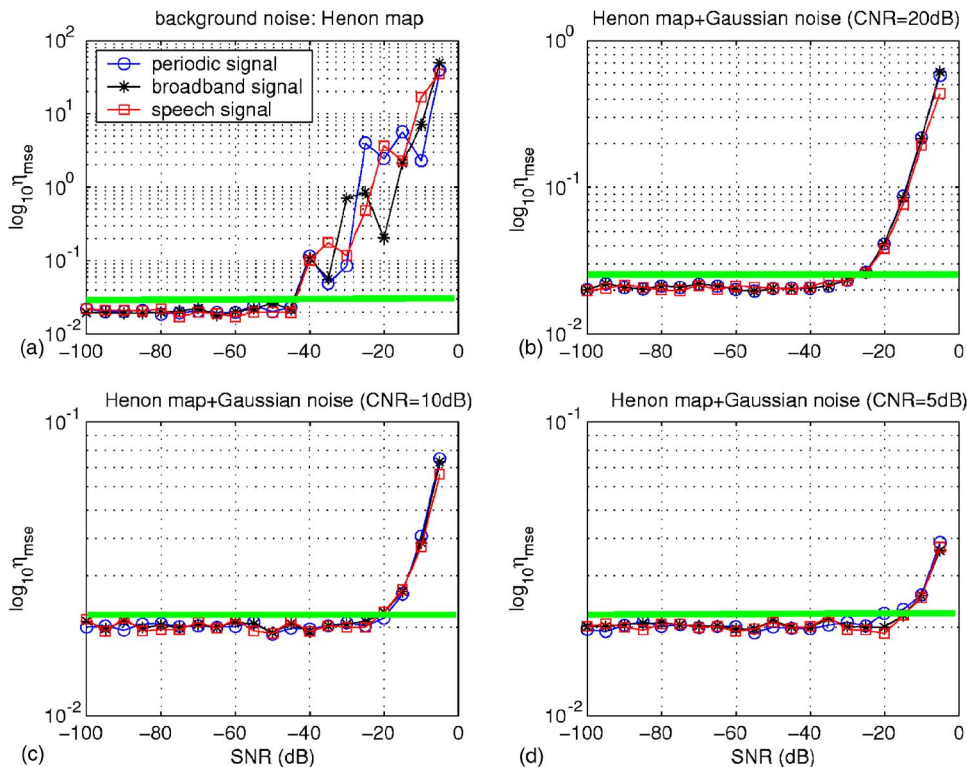
FIG. 6. (Color online) Relative MSE values vs SNR for four different CNR values. The green trace specifies a detection threshold. CNRs are (a) ∞, (b) 20 dB, (c) 10 dB, and (d) 5 dB.
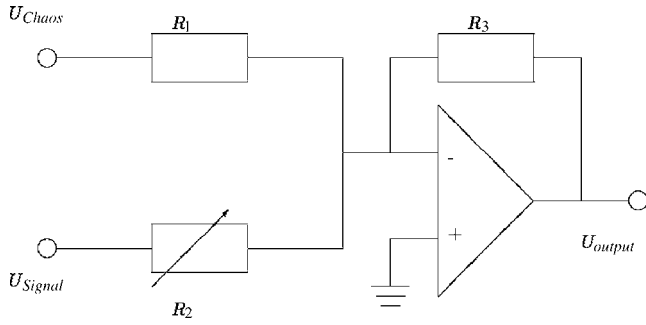
FIG. 7. Circuit diagram for measuring mixed signal. Parameters are R_1 = 10 kΩ and R_3 = 10 kΩ. R_2 is adjustable. Op Amp is $\mu A741CP$.

(SNR ≥ −40 dB). Indeed, Figs. 3(c) and 5(c) illustrate such detection results. Furthermore, with respective CNRs of 20, 10, and 5 dB, Figs. 6(b)–6(d) show that targets can be detected with SNRs larger than −25, −20, and −15 dB, respectively. Therefore, better performance can be expected for relatively higher values of CNR.

IV. APPLICATIONS TO EXPERIMENTAL DATA

A. Chaotic circuit data

In the first experiment, we consider a Lorenz–Stenflo[16,26–28] (LS) chaotic circuit. The circuit equations are given by[27]

$$C_1 \dot{u}_x = -\frac{u_x}{R_{1,5}} + \frac{R_{1,3} u_y}{R_{1,1} R_{1,4}} + \frac{R_{1,3} u_v}{R_{1,2} R_{1,4}},$$

$$C_2 \dot{u}_y = \frac{R_{2,2} u_x}{R_{2,1} R_{2,3}} - \frac{u_y}{R_{2,5}} - \frac{u_x u_z}{R_{2,4}}, \tag{11}$$

$$C_3 \dot{u}_z = \frac{R_{3,2} u_x u_y}{R_{3,1} R_{3,3}} - \frac{u_z}{R_{3,4}}, \quad C_4 \dot{u}_v = -\frac{u_x}{R_{4,1}} - \frac{u_v}{R_{4,2}}.$$

Equations (11) are reduced to the classical Lorenz system when the parameter associated with the flow rotation is set to zero: $R_{1,3}/(R_{1,2}R_{1,4})=0$. We add a periodic signal from a conventional laboratory signal generator to the LS chaotic signal by using a summing amplifier, as shown in Fig. 7. The summed output is given by

$$U_{\text{output}} = -(U_{\text{chaos}} R_3/R_1 + U_{\text{signal}} R_3/R_2).$$

For fixed values of R_1 and R_3, the SNR of the data can be adjusted by changing the value of R_2. Experimentally, $U_{\text{chaos}}(\equiv u_x)$ and U_{signal} are in the unit of volts. The signal U_{output} is recorded via an interface circuit through a microphone attached to the computer with an A/D conversion scheme of sampling rate of 8000 Hz and a 16-bit resolution.

In real situations, the target signal is usually found to vary over a wide dynamic range. A qualitative description of the received signal may fall under one of three likely categories:[8] (1) it consists solely of interference; (2) it consists of a weak target signal plus interference; (3) it consists of a strong target signal plus interference, as shown in Figs.
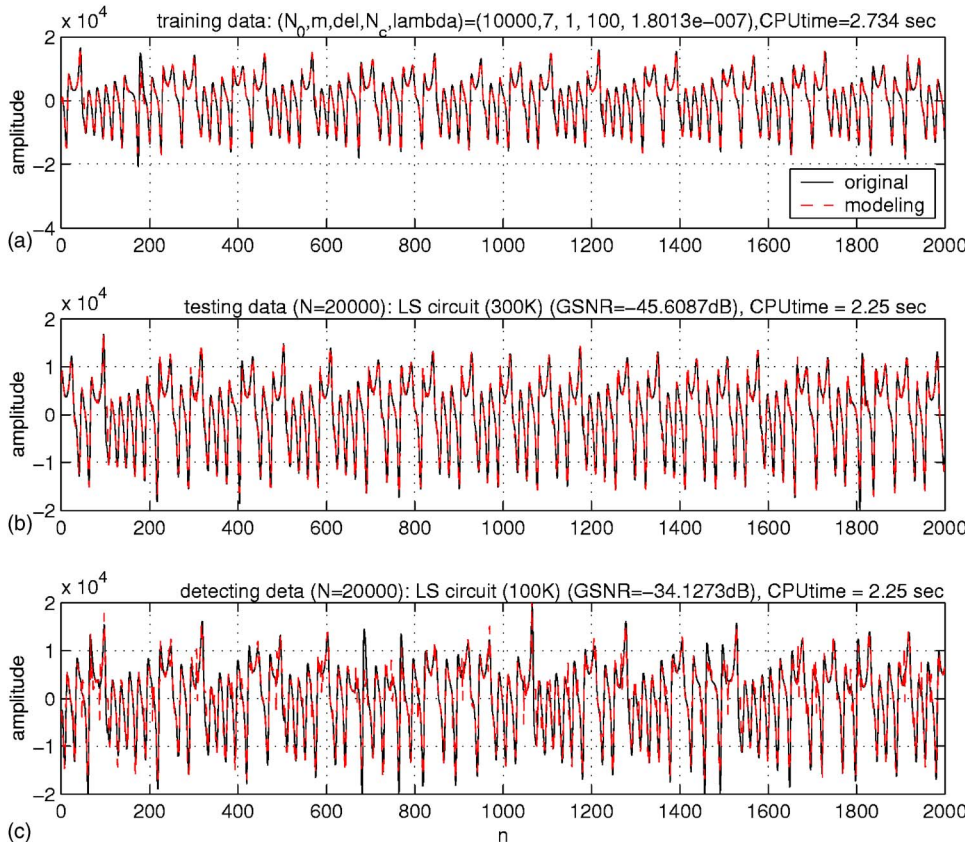

FIG. 8. (Color online) For the LS circuit, (a) chaotic background signal, (b) mixed chaotic and target signal for R_2=300 kΩ, and (c) mixed chaotic and target signal for R_2=100 kΩ. Black trace corresponds to the original time series and red trace (dashed line) corresponds to one-time prediction.
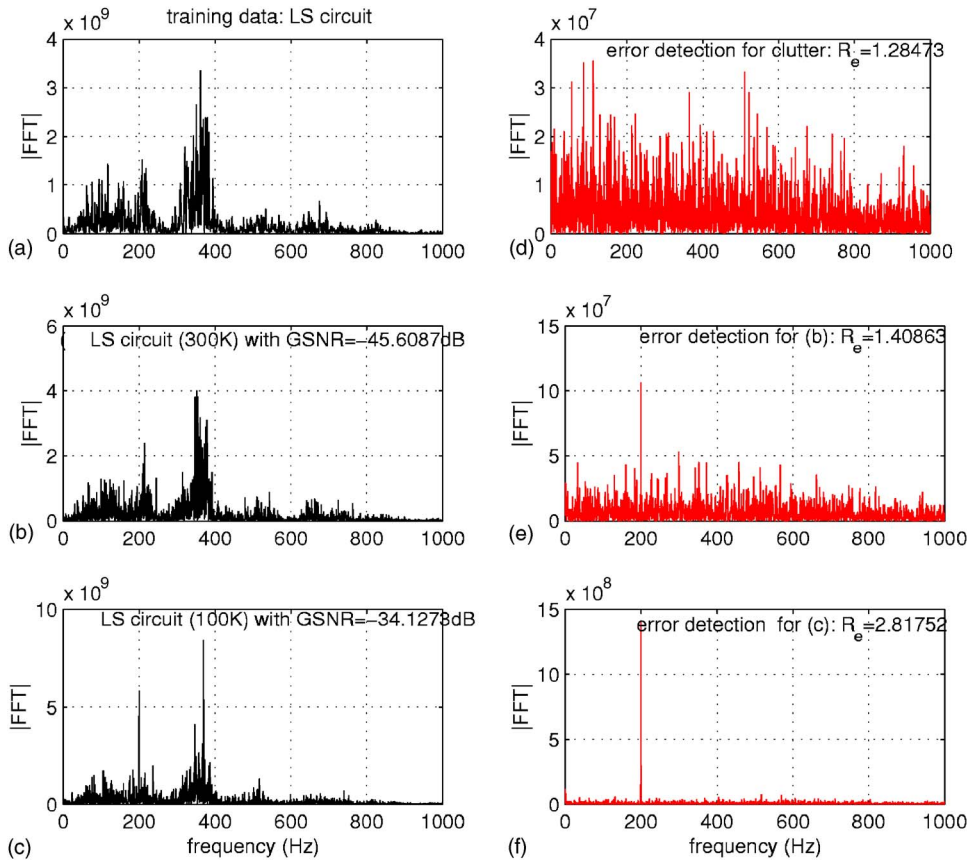
FIG. 9. (Color online) LS chaotic circuit data analyses corresponding to Fig. 8. (a)–(c) Frequency spectra of three measurement data. (d)–(f) Frequency spectra of the detection error.
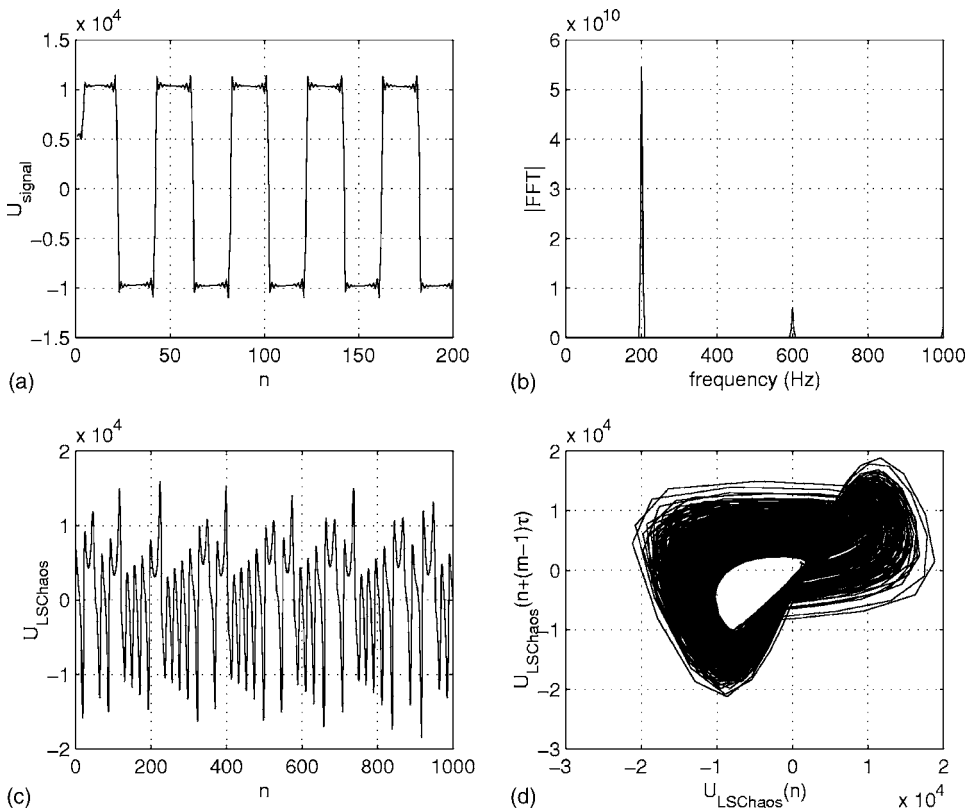

FIG. 10. (a) A target signal, (b) frequency spectrum of the target signal ($f_0 = 200$ Hz), (c) chaotic time series of the LS circuit, and (d) reconstructed phase space of chaotic circuit system with $m = 7$ and $\tau = 13$.
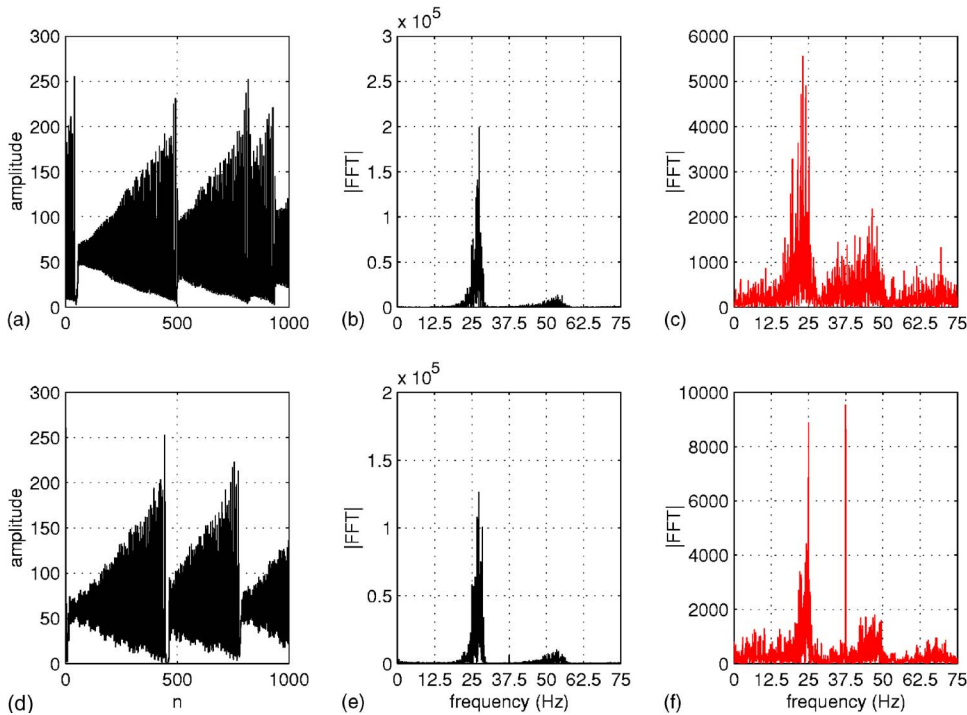
FIG. 11. (Color online) For NH$_3$ laser data, (a) original chaotic background data, (b) frequency spectrum of the signal in (a), (c) frequency spectrum of prediction error signal for (a), (d) mixed chaotic background and target signal, (e) frequency spectrum of the signal in (d), and (f) frequency spectrum of prediction error signal for (d).

8(a)–8(c), respectively. The frequency spectra are plotted in Figs. 9(a)–9(c), respectively. When there is no external input signal U_{signal} [Fig. 10(c)], a nonlinear time-series analysis yields $D_2 \approx 2.61$. We thus choose $m=7$. The time delay is chosen to be[29] $\tau=13$. The corresponding reconstructed phase space is shown in Fig. 10(d).

In RBF-based detection experiments, 10 000 LS circuit time series are used for training, where 100 center points are randomly chosen from the reconstruction attractor. By using the BIC algorithm, the optimal regularization parameter is found to be $\lambda \approx 1.8 \times 10^{-7}$. As soon as the network weight W is trained, the modeling results can be computed by Eq. (1). We found that the trained RBF network is an excellent dynamical model for the chaotic circuit data. By fixing the network parameters, i.e., centers, regularization parameter, and weight, the detection performance of our technique is evaluated by using 20 000 samples from the other two data sets. Figures 9(d)–9(f) show the detection errors. In particular, we use a new data set with 2000 sample points to test the modeling ability of the network. As shown in Fig. 9(d), the frequency spectrum exhibits a white noise spectrum. When the signal is strong [the 200 Hz frequency line seen in Fig. 9(c)], the signal frequency can be extracted accurately, as shown in Fig. 9(f). For a weak signal completely hidden in the chaotic noise spectrum [Fig. 9(b)], our technique is also able to detect the signal frequency, as shown in Fig. 9(e).

B. NH$_3$ laser data

We have also used a chaotic far-infrared-laser data to evaluate our detection scheme. In this case, the dynamical equations that generate the chaotic data are not available. The time series represents the output power of the laser intensity, consisting of 9000 data points. Part of it is shown in Fig. 11(a). Similar to the LS circuit model, the system exhib-

its high-frequency pulsations, with gradually rising amplitude that collapses to small values in relatively short time. The rapid decay of oscillations in this data occurs with no periodicity and is a challenge to model building. During the collapses the signal abruptly jumps from one region of the attractor to another, and these transitions are the most difficult part of the series to model. The corresponding frequency spectrum of the signal is shown in Fig. 11(b).

The embedding parameters are found to be $(m, \tau) = (9, 2)$ for this laser series. The first 3000 samples of data points are employed to train the RBF network, while the second 3000 data points are used to check the prediction ability of the underlying dynamical system. The remaining 3000 data samples are reserved for the purpose of weak signal detection, whereby a periodic signal of two different frequencies are added with a SNR=−22 dB. Comparing Fig. 11(b) with Fig. 11(e), we see that the additional periodic signal is completely hidden in the NH$_3$ laser frequency spectrum. Figure 11(f) is our detection result. Comparing the difference between Figs. 11(f) and 11(c), we see that the two signal frequencies, of 25 and 37.5 Hz, can be extracted faithfully from the mixed data.

V. COMPARISON WITH TRADITIONAL TECHNIQUES OF WEAK SIGNAL DETECTION

By applying our model-based method for different chaotic experimental data sets, we have demonstrated that the technique performs well to detect weak signals. To better evaluate the detection method, we have compared it with two traditional methods of frequency estimation: the standard WPDENCMP denoising wavelet method[30] and supervised principal components analysis (SPCA) detector.[14] To further demonstrate the generality of our method, we use a different
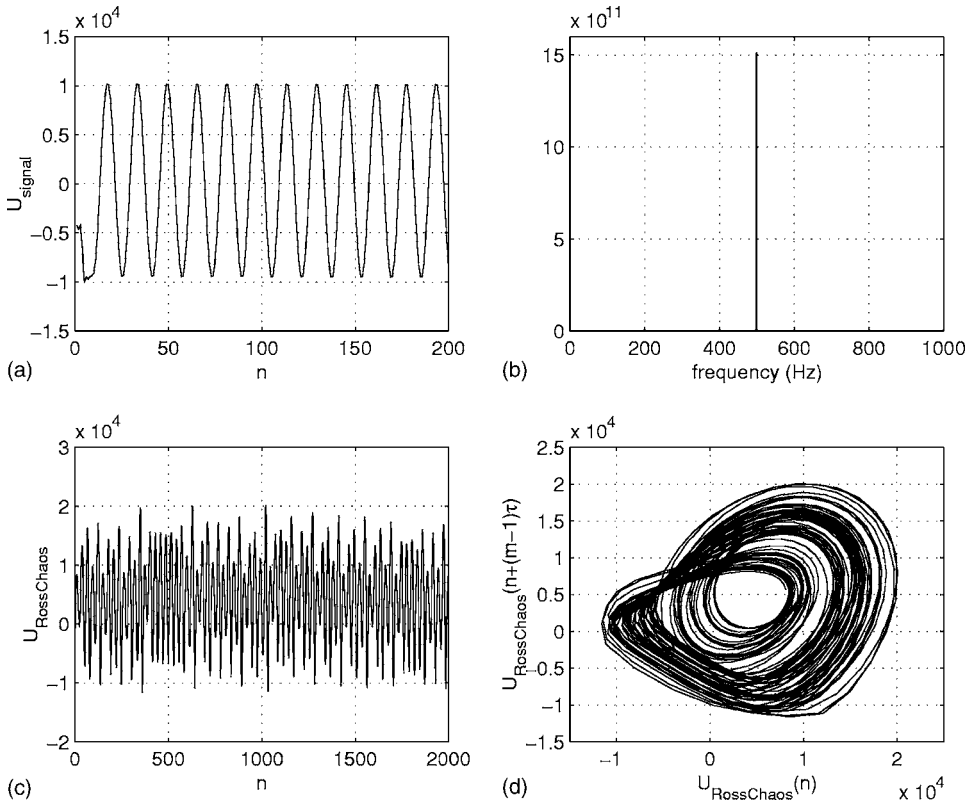
FIG. 12. (a) Target signal $\sin(2\pi f_0 t)$, where $f_0 = 500$ Hz, (b) frequency spectrum of the target signal, (c) background chaotic signal from the Rössler circuit, and (d) reconstructed phase-space plot of the chaotic signal.

set of experimental chaotic signals: chaotic Rössler circuit data, and test all three methods. The circuit simulates a modified version of the Rössler equations, where the quadratic nonlinearity is replaced by a piecewise linear element.[31]

A circuit diagram and equations can be found in Refs. 31 and 32. A target signal [$U_{signal} = \sin(2\pi f_0 t)$ with $f_0 = 500$ Hz], its Fourier spectrum, and a representative chaotic Rössler circuit signal are shown in Fig. 12. A reconstructed phase
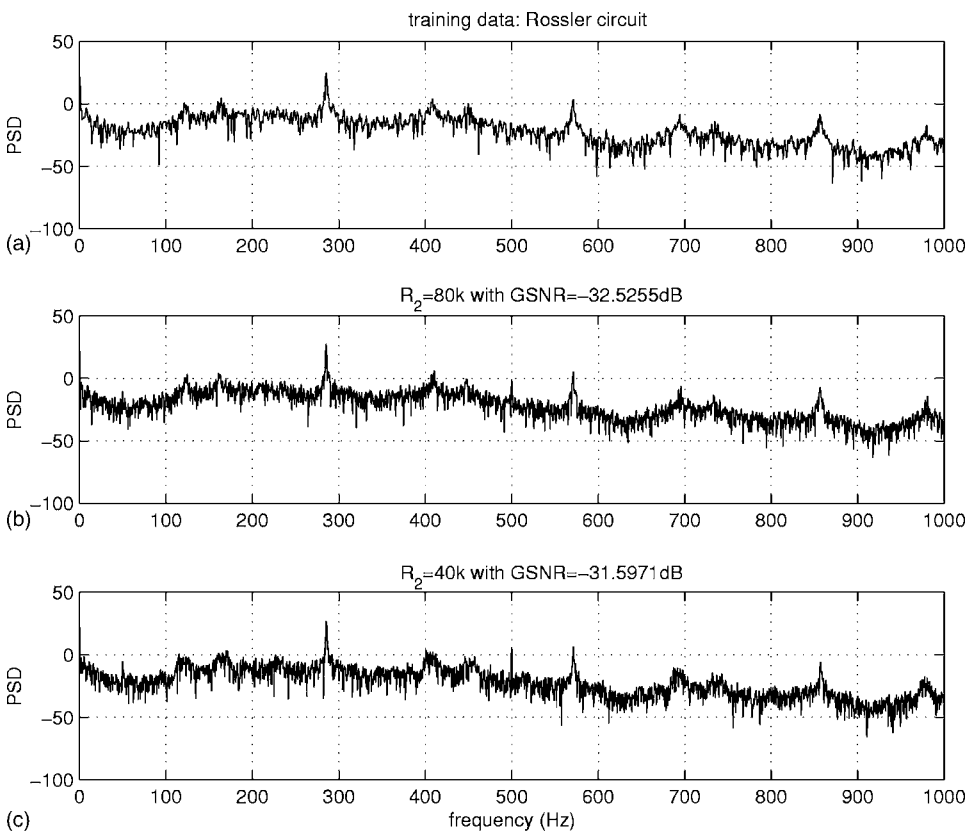

FIG. 13. Frequency spectra of three measurement data from the Rössler circuit: (a) background chaotic signal (b) $R_2 = 80$ kΩ, and (c) $R_2 = 40$ kΩ.
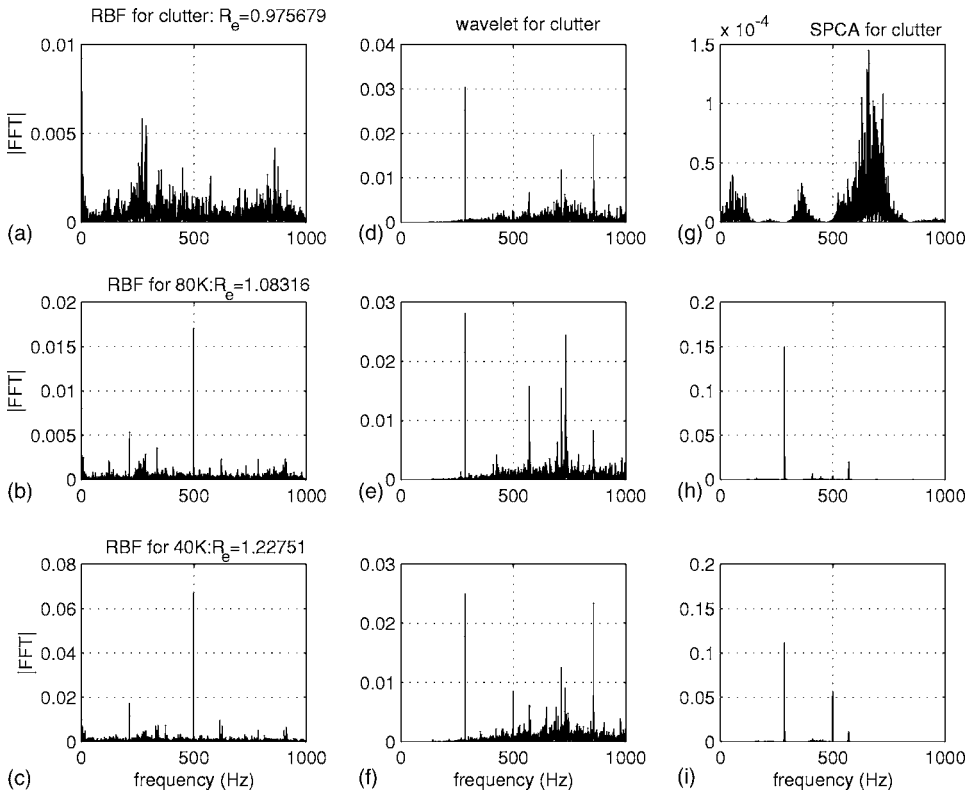
FIG. 14. Frequency spectra of detection error corresponding to three cases in Fig. 13: (a)–(c) from our model-based scheme, (d)–(f) from wavelet denoising, and (g)–(i) from SPCA detector.

space is shown in Fig. 12(d), where the embedding dimension is chosen to be $m=5$ ($D_2 \approx 2.43$) and time delay is $\tau = 6$. We have considered three cases as for the LS circuit data. Figure 13 shows the corresponding frequency spectra. The 500 Hz signal is much weaker than the Rössler signal components at the fundamental frequency $f=285$ Hz and its harmonic frequencies.

To carry out the detection scheme, 10 000 circuit samples are trained, where 100 center points are randomly chosen from the reconstructed attractor. By using the BIC algorithm, the optimal regularization parameter is found to be $\lambda \approx 3.6 \times 10^{-8}$. The detection results are shown in Figs. 14(a)–14(c). When there is no external input signal, the detected error exhibits a white-noise-like spectrum, but it can be seen from Fig. 14(a) that the maximum frequency peak appears at $f=285$ Hz. When the signal is weak, detection results indeed reveal a clear signal frequency line ($f = 500$ Hz), as shown in Figs. 14(b) and 14(c).

We now apply the standard wavelet denoising technique[30] to analyze our three cases. We first apply the function DDENCMP to compute the threshold parameter as well as other coefficients by using the chaotic data. As soon as the parameters are trained, we denoise the test data for ten times by changing the threshold parameter so as to find the optimal detection result. One of the results is shown in Figs. 14(d)–14(f). We note from Fig. 14(e) that the fundamental frequency 285 Hz and its harmonic frequencies of the chaotic time series are extracted, but the additional signal frequency 500 Hz is undetectable. When the signal is strong, the extracted signal frequency has a lower amplitude than other frequency components. Thus, the wavelet-based

method appears not capable of extracting the signal frequency even when the signal is strong.

We next turn to SPCA detection. As discussed in the Ref. 14, there are two channels in an SPCA detector. Each channel consists of a nonlinear phase-space reconstructor (for embedding a data matrix using the received time series in terms of data dimension q and time delay τ) and a principal components analyzer (for feature extraction). The output error time series, which results from the difference between the two sets of eigenvectors of the correlation data matrices from these two channels, is analyzed using the standard frequency estimation. In the detection experiment, we choose the time delay $\tau=1$ and the data dimension $q=20$. The feature dimension can be chosen to be the embedding dimension m. We use $m=5$. The signal frequency extracted is shown in Figs. 14(g)–14(i). When the signal is weak, the signal frequency cannot be extracted correctly, as shown in Fig. 14(h). However, it can be seen from Fig. 14(i) that the SPCA detection algorithm is able to extract the signal frequency line at 500 Hz, although the fundamental frequency 285 Hz of the Rössler chaotic signal is also extracted.

The reason that the detection performance of the wavelet denoising technique or SPCA detector is not as good as the model-based method can be seen as follows. The wavelet packet uses entropy criterion to decompose the signal from noisy data, where a different threshold parameter may give a different decomposition result. If both the signal and the background chaotic signal are of completely different statistical characteristics, the entropy-based decomposition technique can be used, but difficulty arises when the target signal and the chaotic data cannot be distinguished statistically. On

the other hand, the SPCA algorithm uses the feature space to detect small difference between chaotic and mixed signal. An improper choice of parameters could lead to some false frequency peaks. In particular, the generation of this *ghost signal* is due mainly to the slight nonstationarity of the background noise and, to some extent, the use of relatively short data length (10 000 data points used for training) in our experiments as constrained by computational resources. However, the model-based approach uses a neural network to mimic the unknown generating equations of a time series. Therefore, instead of explicitly deducing the equations describing the underlying dynamics of the system, an implicit neural model that approximates the ideal equations is built. Neural networks are attractive for modeling nonlinear dynamical systems because they are inherently nonlinear (due to nonlinear activation functions).[9,20] The model-based scheme is able to capture the dynamical features of the system, enabling weak signals to be detected.

VI. CONCLUSION

In this paper, we have addressed the problem of detecting weak signals in chaotic or random interference environments. By analyzing Hénon chaotic time series as well as experimentally measured data sets, we have shown that a detection scheme, which is based on chaos, nonlinear phase-space reconstruction technique, and RBF neural networks, is capable of detecting weak signals buried in a chaotic noisy background. In particular, the computational time to train the network is fast, making it suitable for real time applications. The scheme therefore represents a useful approach to detection in nonlinear signal processing, and we expect it to be widely applicable for identifying and extracting weak signals buried in strong in-band noise.

ACKNOWLEDGMENTS

[1]D. S. Broomhead and G. P. King, Physica D **20**, 217 (1986).
[2]D. S. Broomhead, J. P. Huke, and R. Jones, Physica D **80**, 413 (1995).
[3]D. S. Broomhead, J. P. Huke, and M. A. S. Potts, Physica D **89**, 439 (1996).
[4]L. M. Pecora, T. L. Carroll, and J. F. Heagy, Phys. Rev. E **52**, 3420 (1995).
[5]L. M. Pecora, L. Moniz, J. Nichols, and T. L. Carroll, Chaos **17**, 013110 (2007).
[6]T. I. Netoff, L. M. Pecora, and S. Schiff, Phys. Rev. E **69**, 017201 (2004).
[7]C. L. Goodridge, L. M. Pecora, T. L. Carroll, and F. J. Rachford, Phys. Rev. E **64**, 026221 (2001).
[8]S. Haykin and X. B. Li, Proc. IEEE **83**, 95 (1995), and references therein.
[9]P. Yee and S. Haykin, IEEE Trans. Signal Process. **47**, 2503 (1999).
[10]S. Haykin and T. K. Bhattacharya, IEEE Trans. Signal Process. **45**, 1619 (1997).
[11]Y. C. Lai, M. G. Frei, I. Osorio, and L. Huang, Phys. Rev. Lett. **98**, 108102 (2007).
[12]K. Park, Y. C. Lai, S. Krishnamoorthy, and A. Kandangath, Chaos **17**, 013105 (2007).
[13]Y. C. Lai, M. G. Frei, and I. Osorio, Phys. Rev. E **73**, 026214 (2006).
[14]C. T. Zhou, T. X. Cai, and T. F. Cai, Chaos **17**, 013108 (2007).
[15]D. Napoletani, D. C. Struppa, T. Sauer, C. A. Berenstein, and D. Walnut, Chaos **16**, 043116 (2006).
[16]T. F. Cai, T. X. Cai, C. T. Zhou, and M. Y. Yu, Phys. Scr. **66**, 187 (2002); **65**, 469 (2002).
[17]K. Fukunaga, *Introduction to Statistical Pattern Recognition*, 2nd ed. (San Diego, Academic, 1990).
[18]F. Takens, Lect. Notes Math. **898**, 366 (1980).
[19]See, for example, H. Kantz and T. Schreiber, *Nonlinear Time Series Analysis* (Cambridge University Press, Cambridge, 1997).
[20]S. Haykin, *Neural Networks, A Comprehensive Foundation* (Macmillan, New York, 1999).
[21]L. Cohen, Proc. IEEE **77**, 941 (1989).
[22]C. T. Zhou and M. Y. Yu, Phys. Scr. **60**, 300 (1999).
[23]M. J. L. Orr, Neural Comput. **7**, 606 (1995).
[24]In our all chaotic data processing, we have taken an initial value of $\lambda = 1$, and have found that it gives a good convergence. Particularly, a very small value of λ clearly indicates that our chaotic circuit laboratory data sets contain a low noise level.
[25]To have an idea of the noise level in chaotic clutter, we here define a chaos-to-noise ratio (CNR) as $\text{CNR(dB)} = 20 \log_{10}[std(\text{chaos})/std(\text{noise})]$, and the SNR is then defined as $\text{SNR(dB)} = 20 \log_{10}[std(\text{signal})/std(\text{chaos}+\text{noise})]$.
[26]L. Stenflo, Phys. Scr. **53**, 83 (1996).
[27]C. T. Zhou, C. H. Lai, and M. Y. Yu, J. Math. Phys. **38**, 5225 (1997).
[28]C. T. Zhou, Phys. Scr. **65**, 25 (2002).
[29]Although the time delay deduced from the mutual information algorithm is 13, we found that for RBF-based detection purpose, a better performance is obtained with $\tau = 1$.
[30]M. Misiti, Y. Misiti, G. Oppenheim, and J. Poggi, *Wavelet Toolbox: For Use With Matlab*® (The Math Works, Natick, MA, 1996–1997).
[31]J. F. Heagy, T. L. Carroll, and L. M. Pecora, Phys. Rev. E **50**, 1874 (1994).
[32]S. Boccaletti, D. L. Valladares, L. M. Pecora, H. P. Geffert, and T. Carroll, Phys. Rev. E **65**, 035204 (2002).